Journal of Multidisciplinary and Translational Research (JMTR)

journal homepage: https://journals.kln.ac.lk/jmtr/

Feasibility of a convolutional neural network (CNN)-based approach for the detection of *Leishmania* parasites in microscopic fields as an adjunct diagnostic tool for leishmaniasis

J.A.Y.S. Amarathunge[1], N. Gunathilaka[2]*

[1]*Department of Parasitology, Faculty of Medicine, University of Kelaniya, Ragama, Sri Lanka*

Abstract

Leishmaniasis, caused by protozoan parasites of the genus *Leishmania*, is ranked among the top 10 neglected tropical diseases (NTDs) by the World Health Organization and constitutes a significant global public health burden. In Sri Lanka, cutaneous leishmaniasis is the predominant clinical form, and the disease is considered endemic, yet the absence of a national surveillance program and the scarcity of trained microscopists remain critical barriers to timely and accurate diagnosis. Conventional microscopy, while remaining the primary diagnostic standard, is inherently operator-dependent and susceptible to misinterpretation by less experienced personnel. The present study aimed to evaluate the feasibility of a convolutional neural network (CNN)-based deep learning model, built on the TensorFlow framework, for the automated detection of *Leishmania* amastigotes in stained microscopic field images. A dataset comprising 161 microscopic field images, including 91 positive images for *Leishmania* amastigotes and 70 negative images, was used to evaluate model performance. The model correctly classified 88 of 91 positive images (sensitivity: 96.7%) and 65 of 70 negative images (specificity: 92.9%), achieving an overall diagnostic accuracy of 95.0%. The positive predictive value and negative predictive value were 94.6% and 95.6%, respectively. Receiver operating characteristic (ROC) curve analysis demonstrated excellent discriminatory performance, with an area under the curve (AUC) of 0.999. Notably, the model demonstrated the capacity to discriminate *Leishmania* amastigotes from morphologically similar artefacts, including platelet clumps, a recognized source of false-positive diagnoses in routine microscopy. Performance benchmarks were comparable to, and in some instances exceeded, those reported in previous deep learning studies for *Leishmania* parasite detection and other haemoparasite classification tasks. These findings provide compelling evidence for the feasibility of CNN-based automated image analysis as a cost-effective, and accurate adjunct or alternative to conventional microscopy for leishmaniasis diagnosis in resource-limited settings. Validation using larger, geographically diverse datasets and prospective clinical workflow evaluation is recommended as the next step toward clinical implementation.

Keywords: Convolutional neural network, Deep learning, Image classification, *Leishmania*, Leishmaniasis, Machine learning, TensorFlow

Article info

Article history:
Received 10th May 2026
Received in revised form 15th June 2026
Accepted 25th July 2026
Available online 25th August 2026

ISSN (E-Copy): ISSN 3051-5262
ISSN (Hard copy): ISSN 3051-5602
Doi:
ORCID iD: https://orcid.org/0000-0002-2690-8565
*Corresponding author:
E-mail address: n.gunathilaka@kln.ac.lk (N. Gunathilaka)

Introduction

Leishmaniasis is a vector-borne parasitic disease caused by obligate intracellular protozoan parasites of the genus *Leishmania*, transmitted to vertebrate hosts through the bites of infected female phlebotomine sandflies of the family Psychodidae (Mann et al., 2021). The disease is classified by the World Health Organization (WHO) among the top ten neglected tropical diseases (NTDs) targeted for control or elimination, reflecting its disproportionate impact on vulnerable populations worldwide (WHO, 2023). Leishmaniasis manifests in three principal clinical forms: cutaneous leishmaniasis (CL), the most prevalent, causing chronic skin ulcers; visceral leishmaniasis (VL), the most severe, characterized by systemic organ involvement and high case fatality if untreated; and mucocutaneous leishmaniasis (MCL), which causes progressive destruction of the mucosal membranes of the nose and oral cavity (Ready, 2014). Globally, an estimated 12 million people are infected across 99 countries, with approximately 0.7–1.0 million new CL cases and 50,000–90,000 new VL cases reported annually (Mann et al., 2021; WHO, 2023).

In Sri Lanka, CL is the predominant clinical form and has been recognized as an endemic disease, with increasing case notifications from multiple provinces over the past two decades (Karunaweera et al., 2003; Kaluarachchi et al., 2019). The epidemiology of leishmaniasis in Sri Lanka is complicated by the absence of a systematized national surveillance programme; epidemiological monitoring is currently assigned to the Anti-Malaria Campaign, a programme with a historically distinct mandate. This structural gap, compounded by limited research capacity and under-reporting at peripheral health institutions, significantly constrains the accuracy of disease burden estimates. The principal causative agent of CL in Sri Lanka has been identified as *Leishmania donovani*, which unusually manifests cutaneous rather than visceral pathology in the Sri Lankan context, suggesting the existence of a distinct parasite genotype or host–parasite interaction (Siriwardana et al., 2010).

Microscopy-based examination of Giemsa-stained tissue smears or aspirate preparations for *Leishmania* amastigotes remains the primary and most widely accessible diagnostic method in endemic low-income countries (Goto & Lindoso, 2010). Despite its widespread use, conventional microscopy is highly operator-dependent; reported sensitivity ranges from 53% to 98%, with significant variation attributable to differences in slide preparation, staining technique, operator experience, and parasite density in the sample (Goto & Lindoso, 2010; Reithinger & Dujardin, 2007). In Sri Lanka, personnel trained in *Leishmania* microscopy are concentrated in a small number of specialist healthcare institutions; at primary and secondary care levels, the shortage of trained microscopists is a recognized impediment to timely diagnosis (Kaluarachchi et al., 2019). Diagnostic error, including false-negative and false-positive interpretations arising from confusion with morphologically similar structures such as platelet clumps and macrophage nuclei, remains a documented clinical problem (Goto & Lindoso, 2010).

The rapid advancement of artificial intelligence (AI), particularly machine learning (ML) and deep learning (DL) technologies, has opened transformative possibilities for automated image-based diagnostics in biomedical and parasitological sciences (Holmström et al., 2017; Rajaraman et al., 2018). Convolutional neural networks (CNNs) have achieved state-of-the-art performance across a wide range of medical image classification tasks owing to their capacity for hierarchical, data-driven feature extraction without manual feature engineering (LeCun et al., 2015). In the context of parasitological diagnostics, Górriz et al. (2018) employed a U-net-based deep learning

architecture for the segmentation and classification of *Leishmania* parasites, reporting results comparable to expert-level microscopy. Inayah et al. (2020) achieved 95.0% classification accuracy for *Plasmodium falciparum* detection using randomly wired neural networks, and Rajaraman et al. (2018) demonstrated that pre-trained CNNs could achieve high accuracy in malaria parasite detection from thin blood smear images.

Despite these advances, the systematic evaluation of automated ML-based tools for *Leishmania* parasite detection in resource-limited settings, where scalability and operational simplicity are paramount, remains underexplored. Existing deep learning approaches for leishmaniasis have largely been developed in high-income country research environments, with limited attention to deployment feasibility in settings such as Sri Lanka (Calvo-Alvarez et al., 2015). The present study therefore aimed to develop a CNN-based ML model within the TensorFlow framework for the automated binary classification of *Leishmania* amastigotes in stained microscopic field images, evaluate model diagnostic performance on an independent test dataset, and assess feasibility as an alternative or adjunct diagnostic tool for leishmaniasis in low-resource healthcare settings in Sri Lanka.

Methodology

Study design and slide selection

This was a laboratory-based feasibility study conducted at the Department of Parasitology, Faculty of Medicine, University of Kelaniya, Sri Lanka. Archived diagnostic slides previously confirmed positive or negative for *Leishmania* amastigotes by an experienced parasitologist through standard light microscopy of Giemsa-stained tissue preparations were selected. A total of 75 confirmed-positive slides and 75 confirmed-negative slides were included. Slides were selected to represent a range of parasite densities in the positive group, reflecting the spectrum of parasite loads encountered in routine clinical practice.

Image acquisition and dataset construction

From each slide, two representative microscopic field images were captured, yielding 300 images in total: 150 from positive slides and 150 from negative slides. All images were captured at ×100 objective with oil immersion using a binocular compound microscope (Olympus CX23, Japan) equipped with a calibrated digital camera (Olympus SC30). Standardized imaging conditions were maintained, including fixed light intensity, magnification, and camera exposure settings, to minimise inter-image variability. Images were saved in JPEG format at a minimum resolution of 300 dpi. All images were manually reviewed and labelled by a qualified parasitologist prior to model training: class 1 (positive) for fields containing *Leishmania* amastigotes, and class 0 (negative) for parasite-free fields. Full details of the dataset composition are presented in Table 1.

Machine learning model architecture and development

The machine learning model was developed using TensorFlow (version 2.x; Google LLC, Mountain View, CA, USA), an open-source deep learning framework widely used for image-based classification tasks. The model architecture was based on CNNs comprising sequential

convolutional layers with rectified linear unit (ReLU) activation functions, followed by max-pooling layers for spatial down sampling, fully connected dense layers for high-level feature integration, and a final sigmoid activation layer for binary classification output. Dropout regularization was incorporated to reduce the risk of overfitting given the relatively modest training dataset size. The model was configured to support two input modalities: (i) static microscopic field images provided as JPEG or PNG files; and (ii) real-time image analysis from a live microscope-mounted digital camera feed. The model was compiled using the binary cross-entropy loss function and the Adam optimizer.

Table 1: Composition of the microscopic image dataset* used for machine learning model development and independent testing

Dataset component	Positive images (n)	Negative images (n)	Total images (n)
Slides included	75	75	150
Images per slide	2	2	2
Model development dataset	150	150	300
Independent test dataset	91	70	161
Total images	**241**	**220**	**461**

*Positive images: microscopic fields confirmed to contain *Leishmania* amastigotes. Negative images: confirmed to be free of *Leishmania* parasites.

Model training and validation

A total of 300 microscopic field images (150 positive, 150 negative) were used for model training, with the goal of optimising parameters for automated binary classification of microscopic fields as positive or negative for *Leishmania* parasites. Prior to model input, images were resized to 224 × 224 pixels, pixel values were normalized to a range of −1 to +1 using linear scaling, and all images were processed in RGB colour format. The training configuration is summarized in Table 2.

Table 2: Convolutional neural network (CNN) model training configuration

Training parameter	Value
Epochs	50
Batch size	16
Learning rate	0.00101
Final training accuracy	≈100%

Independent model testing and performance evaluation

Performance was evaluated on an independent dataset of 161 microscopic field images (91 positive, 70 negative) not used during model development. Classification outputs were compared against reference labels assigned by expert microscopic examination. A confusion matrix was constructed to quantify true-positive (TP), true-negative (TN), false-positive (FP), and false-negative (FN) classifications. Sensitivity, specificity, positive predictive value (PPV), negative predictive value (NPV), and overall diagnostic accuracy were calculated using standard formulae (Altman & Bland, 1994). The diagnostic odds ratio (DOR) and Youden Index were calculated as

additional discriminatory measures (Glas et al., 2003). Receiver operating characteristic (ROC) curve analysis and area under the curve (AUC) determination were performed (Hanley & McNeil, 1982).

Ethics statement

This study utilized archived diagnostic slides; no patient samples were freshly collected for the purposes of this research and no personally identifiable patient information was accessed or recorded. Ethical approval was not required for this study as it is based on secondary analysis of archived diagnostic material with no direct patient involvement.

Results

Dataset composition

A total of 461 microscopic field images were assembled across the model development (n = 300) and independent evaluation (n = 161) datasets. The development dataset comprised 150 positive and 150 negative images derived from 75 confirmed-positive and 75 confirmed-negative Giemsa-stained slides, producing a balanced binary classification dataset with a 1:1 positive-to-negative ratio. Dataset composition is summarized in Table 1.

Model training performance

Training accuracy increased rapidly during the initial epochs and approached near-perfect performance by approximately epoch 10, remaining stable thereafter. Training loss decreased progressively towards zero, indicating effective learning of features associated with the presence or absence of *Leishmania* amastigotes. A divergence between training and test performance during later epochs suggested a degree of overfitting consistent with the modest training dataset size; however, subsequent evaluation on the independent dataset confirmed that the model retained strong discriminatory capability.

Classification of the independent test set

Classification performance on the independent dataset (n = 161) is presented in Table 3 and illustrated in Figure 1. Of the 91 positive images, 88 were correctly classified as positive (TP = 88) and three were incorrectly classified as negative (FN = 3). Of the 70 negative images, 65 were correctly classified as negative (TN = 65) and five were incorrectly classified as positive (FP = 5). In total, 153 of 161 images were correctly classified.

Table 3: Confusion matrix for the CNN-based machine learning model evaluated on the independent test set (n = 161)

	Predicted positive	**Predicted negative**
Actual positive (n = 91)	True positive = 88	False negative = 3
Actual negative (n = 70)	False positive = 5	True negative = 65

CNN: convolutional neural network.

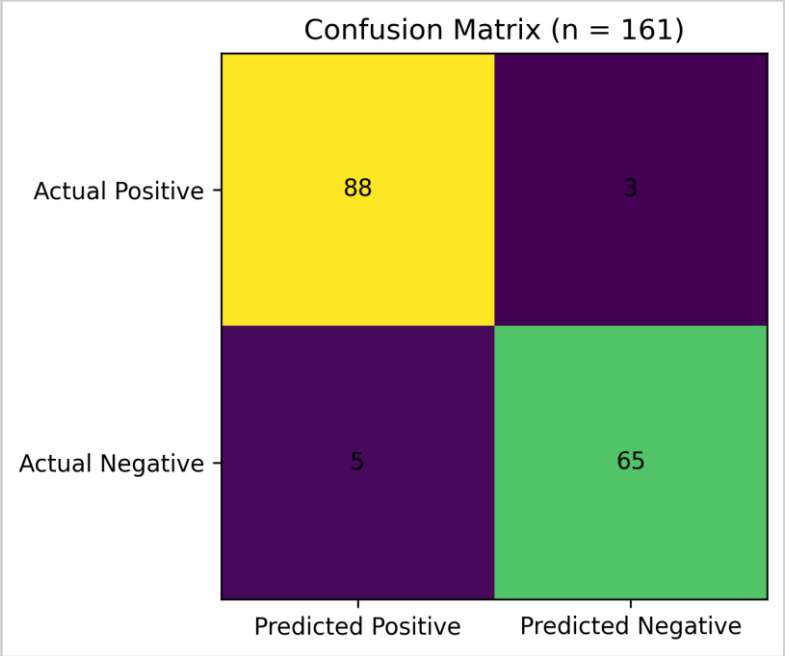

Figure 1. Confusion matrix of the CNN-based machine learning model evaluated on the independent dataset (n = 161). The model correctly classified 88 of 91 *Leishmania*-positive images (true positives) and 65 of 70 parasite-negative images (true negatives), resulting in three false-negative and five false-positive classifications. Overall, 153 of 161 images were correctly classified (accuracy 95.0%).

Diagnostic performance metrics

The full suite of diagnostic performance metrics is presented in Table 4. The model achieved sensitivity of 96.7% (88/91) and specificity of 92.9% (65/70). PPV was 94.6% (88/93), and NPV was 95.6% (65/68). Overall diagnostic accuracy was 95.0% (153/161). The DOR was 381.3, indicating excellent discriminatory performance independent of disease prevalence (Glas et al., 2003), and the Youden Index was 0.896.

Table 4: Diagnostic performance metrics of the CNN-based machine learning model for the detection of *Leishmania* amastigotes in the independent evaluation dataset (n = 161)

Performance metric	n/N*	Value
Sensitivity	88/91	96.7%
Specificity	65/70	92.9%
Positive predictive value (PPV)	88/93	94.6%
Negative predictive value (NPV)	65/68	95.6%
Overall diagnostic accuracy	153/161	95.0%
Diagnostic odds ratio (DOR)	—	381.3
Youden Index (J)	—	0.896
F1-score	—	95.7%
Balanced accuracy	—	94.8%

*n/N: number correctly classified / total in that class. TP: true positive; TN: true negative; FP: false positive; FN: false negative.

ROC curve analysis

ROC curve analysis (Figure 2) demonstrated an AUC of 0.999, indicating near-perfect overall discriminatory performance (Hanley & McNeil, 1982). At the selected operating threshold, the model achieved sensitivity of 96.7% and specificity of 92.9%, demonstrating a favourable balance between false-positive and false-negative classifications.

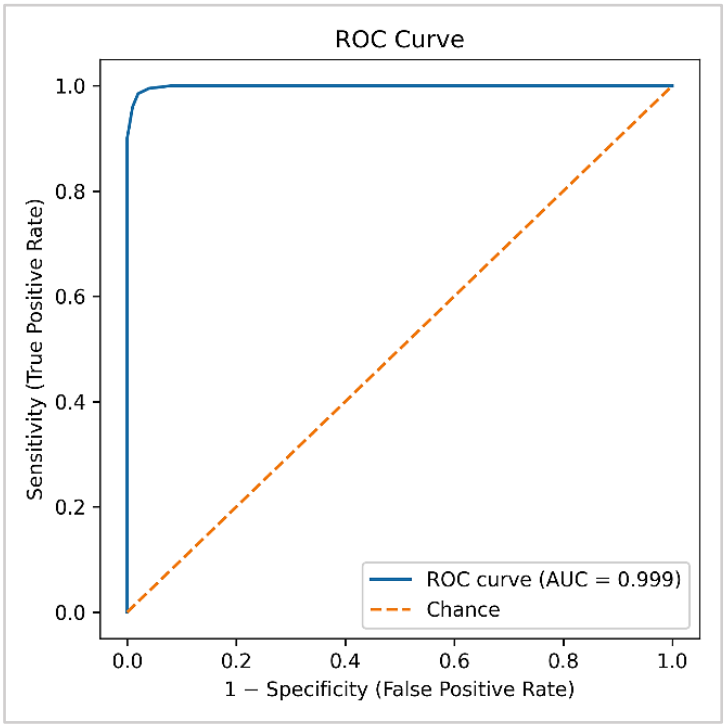

Figure 2. Receiver operating characteristic (ROC) curve for the CNN-based *Leishmania* amastigote detection model evaluated on the independent dataset (n = 161). The solid curve represents model performance; the diagonal dashed line represents chance-level discrimination (AUC = 0.5). AUC = 0.999 indicates near-perfect discriminatory performance.

Characteristics of misclassified images

Eight images were misclassified in the independent evaluation dataset, comprising three false-negative and five false-positive classifications. Representative examples of correctly and incorrectly classified images are illustrated in Figure 3. Review of the false-negative images indicated that low parasite density was the most plausible contributor to misclassification; in these fields, *Leishmania* amastigotes occupied only a small proportion of the total microscopic field, reducing the morphological signal available for CNN-based classification, consistent with patterns reported in previous machine learning studies involving microscopic parasite detection (Rajaraman et al., 2018). The five false-positive classifications occurred in parasite-negative fields containing staining patterns and cellular structures sharing visual characteristics with *Leishmania* amastigotes.

Among the 70 negative images, five fields contained platelet clumps; all five were correctly classified as negative for *Leishmania* parasites. This discriminatory performance suggests that the CNN encoded morphological attributes distinguishing *Leishmania* amastigotes from platelet aggregates, potentially including differences in size, shape, staining characteristics, and surrounding cellular context. The kinetoplast, a distinctive DNA-containing organelle of *Leishmania* amastigotes absent in platelets (Ready, 2014), may also have contributed to the discriminative features learned by the model. This capability is of direct clinical relevance, as platelet clump misidentification is a recognized source of false-positive diagnosis in routine microscopy (Goto & Lindoso, 2010).

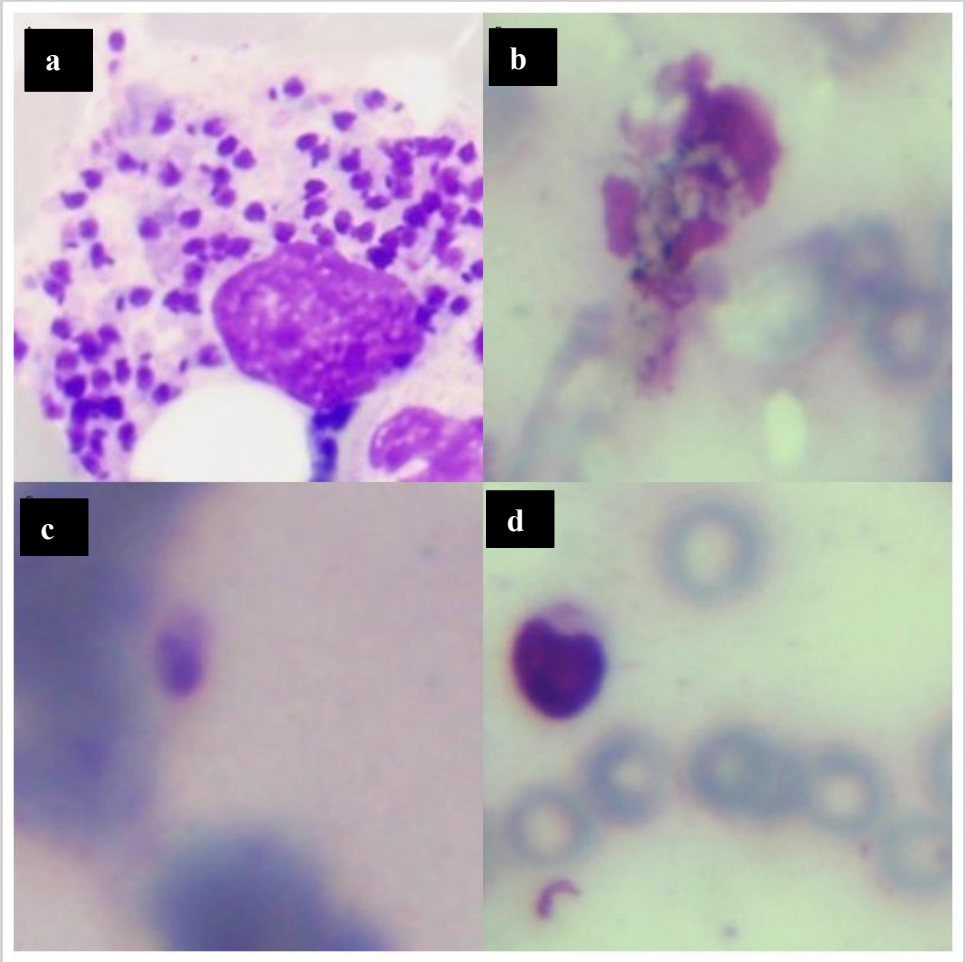

Figure 3. Representative microscopic field images from the independent evaluation dataset. Panel (a): *Leishmania*-positive field correctly classified as positive, showing multiple intracellular amastigotes. Panel (b): parasite-negative field containing a platelet clump, correctly classified as negative. Panel (c): *Leishmania*-positive field misclassified as negative, showing very low parasite burden. Panel (d): parasite-negative field misclassified as positive, containing a densely staining structure morphologically resembling a parasite. Giemsa stain; original magnification ×100 oil immersion.

Comparative diagnostic performance

A comparison of key diagnostic performance metrics against selected published ML and deep learning studies for haemoparasite image classification is presented in Table 5. These

comparisons are presented for context only; the studies differ in target parasite, dataset size and provenance, imaging conditions, model architecture, and in the case of Górriz et al. (2018) task (pixel-wise segmentation rather than binary image classification), so accuracy figures are not directly comparable across studies, and no claim of superiority is intended. The overall diagnostic accuracy of 95.0% achieved in the present study is broadly in line with published benchmarks for CNN-based haemoparasite detection. Inayah et al. (2020) reported 95.0% accuracy using a randomly wired neural network for *Plasmodium falciparum* classification, and Rajaraman et al. (2018) reported sensitivities exceeding 95% using pre-trained CNNs for malaria parasite detection. Comparable performance despite the modest training dataset size suggests that further gains may be achieved through dataset expansion and transfer learning from larger pre-trained networks.

Table 5: Comparative diagnostic performance of the present CNN-based model against selected published machine learning studies for haemoparasite image classification

Study	Target parasite	Method	Dataset	Sensitivity	Specificity	Accuracy
Present study	*Leishmania* amastigotes	CNN (TensorFlow)	300 train / 161 test	96.7%	92.9%	95.0%
Górriz et al. (2018)	*Leishmania* amastigotes	U-net	NR†	NR†	NR†	NR†
Inayah et al. (2020)	*Plasmodium falciparum*	Wired NN	NR	NR	NR	95.0%
Rajaraman et al. (2018)	*Plasmodium* spp.	Pre-trained CNN	>10,000	>95%	>95%	>95%

†Górriz et al. (2018) reported segmentation quality metrics (Dice coefficient, Jaccard index) rather than binary classification accuracy; direct numerical comparison is not applicable. CNN: convolutional neural network; NN: neural network; NR: not reported

Discussion

This study demonstrates that a CNN-based ML model developed within the TensorFlow framework, trained on 300 microscopic field images, achieves excellent diagnostic performance for the automated detection of *Leishmania* amastigotes: sensitivity 96.7%, specificity 92.9%, overall accuracy 95.0%, and AUC 0.999 on an independent evaluation dataset (n = 161). These results substantiate the hypothesis that automated image classification represents a technically feasible and operationally practical adjunct to conventional microscopy for leishmaniasis diagnosis, particularly in healthcare settings where trained diagnostic personnel are scarce.

The diagnostic accuracy achieved is broadly consistent with, though not directly comparable to, published ML-based studies for haemoparasite detection, given differences in target organism, dataset composition, and task across studies. Górriz et al. (2018) developed a U-net segmentation model for *Leishmania* parasites, reporting results comparable to expert-level microscopy using a computationally intensive pixel-wise segmentation approach. The present approach, framing diagnosis as binary image-level classification rather than pixel-wise segmentation, offers a computationally simpler and more readily deployable solution for resource-constrained laboratories. Inayah et al. (2020) achieved approximately 95.0% accuracy for *Plasmodium*

falciparum classification using randomly wired neural networks; the equivalent accuracy achieved here using a conventional CNN architecture underlines the appropriateness of the model design. Rajaraman et al. (2018) reported sensitivities exceeding 95% using pre-trained CNNs for malaria parasite detection, suggesting that the present model's performance may be further improved through the application of transfer learning using large pre-trained image classification networks such as VGG-16, ResNet, or InceptionV3.

The operational design of the model, configured for standard digital microscopic images, enhances practical utility in clinical laboratory settings. Most diagnostic laboratories at secondary and tertiary care institutions in Sri Lanka are equipped with standard compound microscopes with camera attachments; the model's hardware requirements are therefore compatible with existing infrastructure, obviating the need for costly specialized imaging systems. This compatibility with existing infrastructure is a key enabling factor for deployment in the resource-limited settings for which the tool is intended.

Several limitations require acknowledgement. The training dataset of 300 images derived from 150 slides is relatively small by contemporary deep learning standards. Although excellent performance on the independent evaluation dataset was demonstrated, the limited dataset size may constrain model generalizability, and larger datasets incorporating images from multiple healthcare facilities, staining batches, and image acquisition conditions will be required. All images were derived from a single institutional slide archive, meaning imaging conditions and staining protocols remained relatively homogeneous; external validation using image collections from independent laboratories is essential before clinical deployment. No formal head-to-head comparison with expert microscopist performance was conducted, which would provide the most clinically meaningful assessment of the model's diagnostic utility relative to the current standard of care.

Several aspects of the computational training configuration were also not systematically documented at the time of model development and are noted here as limitations on exact reproducibility. The random seed used for weight initialization and data shuffling was not recorded, precluding exact replication of the stochastic elements of training. Detailed per-epoch training and validation accuracy and loss curves were not retained beyond the summary metrics reported in Table 2. The exact minor version of TensorFlow used in the analysis environment was not logged. The process by which the learning rate (0.00101) was arrived at was not formally documented, so it cannot be established with certainty whether this reflected a predetermined default or an informal tuning procedure. These gaps limit exact computational reproducibility, although they do not affect the diagnostic performance metrics reported, which were computed directly from the model’s classification outputs on the independent test set.

Future work should prioritize dataset expansion through multi-site image collection and data augmentation strategies, the application of transfer learning from large pre-trained image classification networks, and prospective external validation in clinical laboratory settings at multiple levels of the Sri Lankan healthcare system. The modular TensorFlow-based architecture of the model also presents opportunities for retraining or fine-tuning for the detection of other parasitic diseases of public health significance in Sri Lanka, including *Plasmodium* species, filarial parasites, and intestinal helminths, where microscopy-based diagnosis similarly suffers from operator dependence and shortages of trained personnel.

Conclusions

This study provides proof of concept for the feasibility of a CNN-based machine learning model for the automated detection of *Leishmania* amastigotes in stained microscopic field images. The model achieved sensitivity of 96.7%, specificity of 92.9%, PPV of 94.6%, NPV of 95.6%, overall diagnostic accuracy of 95.0%, and AUC of 0.999 on an independent evaluation dataset. These results are broadly consistent with published ML and deep learning benchmarks for haemoparasite detection, noting that direct numerical comparison across studies is limited by differences in target organism, dataset, and task. Compatibility with standard laboratory microscope–camera infrastructure positions the model as a scalable, cost-effective adjunct to conventional microscopy for leishmaniasis diagnosis in resource-limited settings such as Sri Lanka. Validation using larger, geographically diverse, and externally sourced image datasets remains essential before clinical implementation and will be critical for establishing generalizability and facilitating eventual integration into diagnostic workflows and national disease surveillance programmes.

Acknowledgements

The authors gratefully acknowledge the technical staff of the Department of Parasitology, Faculty of Medicine, University of Kelaniya, Sri Lanka, for their assistance with slide archiving and image acquisition during the study.

Declaration of Funding Sources

This work was supported by the Research Council, University of Kelaniya, Sri Lanka (Grant No. RC/SROG/2021/03).

Conflict of interest statement

The author declares no conflict of interest.

Data availability statement

The image dataset and model code underlying this study are available from the corresponding author upon reasonable request, subject to institutional ethical approval and data sharing agreement.

Author Contribution

The author was responsible for the conceptualization, methodology, data collection, data analysis, interpretation of results, writing, and revision of the manuscript. The author read and approved the final version of the manuscript.

References

Altman, D.G., & Bland, J.M. (1994). Diagnostic tests 1: Sensitivity and specificity. BMJ, 308(6943), 1552. https://doi.org/10.1136/bmj.308.6943.1552

Calvo-Álvarez, E., Stamatakis, K., Punzón, C., Álvarez-Velilla, R., Tejería, A., Escudero-Martínez, J. M., Pérez-Pertejo, Y., Fresno, M., Balaña-Fouce, R., & Reguera, R. M. (2015). Infrared fluorescent imaging as a potent tool for in vitro, ex vivo and in vivo models of visceral leishmaniasis. *PLoS Neglected Tropical Diseases, 9*(3), e0003666. https://doi.org/10.1371/journal.pntd.0003666

Glas, A.S., Lijmer, J.G., Prins, M.H., Bonsel, G.J., & Bossuyt, P.M. (2003). The diagnostic odds ratio: A single indicator of test performance. Journal of Clinical Epidemiology, 56(11), 1129–1135. https://doi.org/10.1016/S0895-4356(03)00177-X

Górriz, M., Aparicio, A., Raventós, B., Vilaplana, V., Sayrol, E., & López-Codina, D. (2018). Leishmaniasis parasite segmentation and classification using deep learning. In F. J. Perales & J. Kittler (Eds.), *Articulated motion and deformable objects* (pp. 53–62). Springer. https://doi.org/10.1007/978-3-319-94544-6_6

Goto, H., & Lindoso, J.A.L. (2010). Current diagnosis and treatment of cutaneous and mucocutaneous leishmaniasis. Expert Review of Anti-infective Therapy, 8(4), 419–433. https://doi.org/10.1586/eri.10.19

Hanley, J.A., & McNeil, B.J. (1982). The meaning and use of the area under a receiver operating characteristic (ROC) curve. Radiology, 143(1), 29–36. https://doi.org/10.1148/radiology.143.1.7063747

Holmström, O., Linder, N., Ngasala, B., Mårtensson, A., Linder, E., Lundin, M., Moilanen, H., Suutala, A., Diwan, V., & Lundin, J. (2017). Point-of-care mobile digital microscopy and deep learning for the detection of soil-transmitted helminths and *Schistosoma haematobium*. *Global Health Action, 10*(sup3), 1337325. https://doi.org/10.1080/16549716.2017.1337325

Inayah, N., Liebenlito, M., Fitriyati, N., & Monardo, K. (2020). Classification of falciparum parasite in human red blood cells using randomly wired neural network. In 2020 8th International Conference on Cyber and IT Service Management (CITSM) (pp. 1-4). IEEE. https://doi.org/10.1109/CITSM50537.2020.9268806

Kaluarachchi, T. D. J., Weerasekera, M. M., McBain, A. J., Ranasinghe, S., Wickremasinghe, R., Yasawardene, S., Jayanetti, N., & Wickremasinghe, R. (2019). Diagnosing cutaneous leishmaniasis using fluorescence in situ hybridization: The Sri Lankan perspective. *Pathogens and Global Health, 113*(4), 180–190. https://doi.org/10.1080/20477724.2019.1650228

Karunaweera, N. D., Pratlong, F., Siriwardane, H. V. Y. D., Ihalamulla, R. L., & Dedet, J. P. (2003). Sri Lankan cutaneous leishmaniasis is caused by *Leishmania donovani* zymodeme MON-37. *Transactions of the Royal Society of Tropical Medicine and Hygiene, 97*(4), 380–381. https://doi.org/10.1016/S0035-9203(03)90061-7

LeCun, Y., Bengio, Y., & Hinton, G. (2015). Deep learning. *Nature, 521*(7553), 436–444. https://doi.org/10.1038/nature14539

Mann, S., Frasca, K., Scherrer, S., Henao-Martínez, A.F., Newman, S., Ramanan, P., & Suarez, J.A. (2021). A review of leishmaniasis: Current knowledge and future directions. *Current Tropical Medicine Reports, 8*(2), 121–132. https://doi.org/10.1007/s40475-021-00232-7

Rajaraman, S., Antani, S.K., Poostchi, M., Silamut, K., Hossain, M.A., Maude, R.J., Jaeger, S., & Thoma, G.R. (2018). Pre-trained convolutional neural networks as feature extractors

toward improved malaria parasite detection in thin blood smear images. *PeerJ, 6*, e4568. https://doi.org/10.7717/peerj.4568

Ready, P.D. (2014). Epidemiology of visceral leishmaniasis. *Clinical Epidemiology, 6*, 147–154. https://doi.org/10.2147/CLEP.S44267

Reithinger, R., & Dujardin, J.-C. (2007). Molecular diagnosis of leishmaniasis: Current status and future applications. *Journal of Clinical Microbiology, 45*(1), 21–25. https://doi.org/10.1128/JCM.02029-06

Siriwardana, H.V.Y.D., Thalagala, N., & Karunaweera, N.D. (2010). Clinical and epidemiological studies on the cutaneous leishmaniasis caused by *Leishmania (Leishmania) donovani* in Sri Lanka. *Annals of Tropical Medicine and Parasitology, 104*(3), 213–223. https://doi.org/10.1179/136485910x12647085215615

World Health Organization. (2023). Leishmaniasis: Key facts. https://www.who.int/news-room/fact-sheets/detail/leishmaniasis